



Field investigation of volcanic deposits on Vulcano, Italy using a handheld laser-induced breakdown spectroscopy instrument

Kristin Rammelkamp, Susanne Schröder, Gianluigi Ortenzi, Alessandro Pisello, Katrin Stephan, Mickael Baqué, Heinz-Wilhelm Hübers, Olivier Forni, Frank Sohl, Laurenz Thomsen, et al.

► To cite this version:

Kristin Rammelkamp, Susanne Schröder, Gianluigi Ortenzi, Alessandro Pisello, Katrin Stephan, et al.. Field investigation of volcanic deposits on Vulcano, Italy using a handheld laser-induced breakdown spectroscopy instrument. *Spectrochimica Acta Part B: Atomic Spectroscopy*, 2021, 177, 10.1016/j.sab.2021.106067 . insu-03672452

HAL Id: insu-03672452

<https://insu.hal.science/insu-03672452>

Submitted on 3 Feb 2023

HAL is a multi-disciplinary open access archive for the deposit and dissemination of scientific research documents, whether they are published or not. The documents may come from teaching and research institutions in France or abroad, or from public or private research centers.

L'archive ouverte pluridisciplinaire **HAL**, est destinée au dépôt et à la diffusion de documents scientifiques de niveau recherche, publiés ou non, émanant des établissements d'enseignement et de recherche français ou étrangers, des laboratoires publics ou privés.



Distributed under a Creative Commons Attribution - NonCommercial 4.0 International License

Field investigation of volcanic deposits on Vulcano, Italy using a handheld laser-induced breakdown spectroscopy instrument

Kristin Rammelkamp^{a,b}, Susanne Schröder^{a,b}, Gianluigi Ortenzi^{c,d},
Alessandro Pisello^e, Katrin Stephan^c, Mickael Baqué^c, Heinz-Wilhelm
Hübers^{a,f}, Olivier Forni^b, Frank Sohl^c, Laurenz Thomsen^g, Vikram
Unnithan^g

^a*Deutsches Zentrum für Luft- und Raumfahrt (DLR), Institut für Optische
Sensorsysteme, Berlin, Germany*

^b*Institut de Recherche en Astrophysique et Planétologie, Toulouse, France*

^c*Deutsches Zentrum für Luft- und Raumfahrt (DLR), Institut für Planetenforschung,
Berlin, Germany*

^d*Freie Universität Berlin, Department of Earth Sciences, Berlin, Germany*

^e*University of Perugia, Department of Physics and Geology, Perugia, Italy*

^f*Humboldt-Universität zu Berlin, Department of Physics, Berlin, Germany*

^g*Jacobs University Bremen, Department of Physics and Earth Sciences, Bremen,
Germany*

Abstract

Laser-induced breakdown spectroscopy (LIBS) is an important analytical technique in a variety of fields ranging from in-situ terrestrial geological field investigations to robotic exploration missions of extraterrestrial bodies such as Mars. In this study, the performance of a commercial handheld LIBS instrument was evaluated during an international summer school in 2019 that focused on the exploration of extreme environments on Earth and in space. Several sites on the Eolian island Vulcano (Italy) were investigated with different spectroscopic methods including LIBS. We focus here on the exploration of one particular outcrop with LIBS, where layered and colored ash deposits were observed. Furthermore, a laboratory study was performed

Preprint submitted to Journal Name

December 18, 2020

to investigate and validate the effect of varying distance of the instrument to the sample. Unsupervised principal component analysis (PCA) for data exploration showed that elemental variations between the layers of the outcrop can be observed with the LIBS data from the handheld instrument. This was further confirmed by a layer-by-layer analysis of elemental correlations and depositional trends. Geologically relevant major elements such as Si, Al, Ca, Fe, K, Mg, and Na could be identified but also minor and trace elements such as F, Li, Mn, and Sr. Our results also show that the effects of varying distances of the instrument to the sample are critical for the quality of the data acquired and hence pose significant challenges to the analysis and interpretation. We propose a dedicated data pre-processing approach, which includes the masking of emission lines of Ar from the locally induced Ar atmosphere, as a possible solution to overcome this challenge. Overall, this study provides a better understanding of the performance and limitations of a handheld LIBS instrument, particularly in the context of future terrestrial and planetary field investigations.

Keywords: LIBS, portable, in-field, elemental analysis, geochemical, ash layers

1. Introduction

For fast multi-elemental analysis, laser-induced breakdown spectroscopy (LIBS) is a powerful technique in various fields and applications [1], for example, in the steel [2] and nuclear industry [3], in food analysis [4], and in cultural heritage [5]. Another important application of LIBS is the geochemical analysis of samples in laboratories or samples in their geological context

7 in the field [6–8]. Geomaterial analysis in the field extends even to applica-
8 tions beyond Earth and LIBS gains more and more relevance for applications
9 during the robotic exploration of extraterrestrial bodies. The first LIBS in-
10 strument for space exploration is the ChemCam instrument [9, 10], which
11 is part of the scientific payload of NASA’s Mars Science Laboratory (MSL),
12 also known as Curiosity, and which has been analyzing the Martian surface
13 since its landing in 2012 in Gale crater [11].

14 The LIBS technique is sensitive to atmospheric conditions where in par-
15 ticular the thin atmosphere at Mars’ surface (7 mbar of mainly CO₂) is close
16 to ideal for LIBS analysis [12]. There will be an enhanced follow-up in-
17 strument to ChemCam called SuperCam on NASA’s Mars 2020 mission [13]
18 and other LIBS instruments are planned and proposed for the exploration of
19 different extraterrestrial objects [14–18]. Planetary exploration using LIBS
20 instruments is envisaged for in-situ geochemical analysis of superficial rocks
21 and soils in order to reconstruct the geological history of a particular site on
22 the extraterrestrial body, similar to geochemical investigations on Earth.

23 Compared with other analytical methods, the strength of the LIBS tech-
24 nique lies in its instrumental simplicity, apparent ease of use, and versa-
25 tility. For LIBS, a pulsed high-power laser is focused onto the surface of
26 the target resulting in the ablation of material which further evolves into
27 a micro-plasma. Excited atoms, ions, and simple molecules in the plasma
28 emit a characteristic radiation from which the elemental composition of the
29 target can be derived by spectral analysis [19]. In general, the irradiance
30 threshold for the breakdown depends on the material properties but for solid
31 targets an irradiance of $\approx 1 \text{ GW cm}^2$ is considered to produce stable LIBS

32 plasmas suited for analysis [20, 8]. Usually, only optical access is necessary
33 for analyzing samples with LIBS and sample preparation is not mandatory,
34 nevertheless, LIBS results can be substantially improved by using dedicated
35 sample preparation strategies [21, 6, 22]. But still, the possibility to measure
36 without the need for sample preparation makes LIBS especially useful for
37 applications where samples are difficult to access, or where targets are to be
38 analyzed in their original context or when a particularly quick analysis is
39 required.

40 Besides its high ease of use, the LIBS technique has several advantages
41 for geochemical in-situ investigations. For example, while light elements with
42 atomic number < 6 are challenging to detect with other elemental analysis
43 methods such as electron micro probe [23] or alpha particle x-ray spectrom-
44 etry [24], LIBS is sensitive to all elements including H. Furthermore, all ele-
45 ments can be simultaneously detected in real time which enables fast on-site
46 multi-elemental analysis. The sampling area of LIBS instruments depends
47 on the laser spot size on the sample surface which is usually in the range of
48 50-300 μm . This allows to detect changes in the elemental composition and
49 therefore mineral variations on a small scale, and to investigate even small
50 sized grains and features. The capability of using LIBS in the field with-
51 out the need to collect samples, is a great benefit of LIBS for geochemical
52 analysis [8, 6].

53 Nevertheless, the LIBS technique has also some challenges. These arise
54 mainly from the sensitivity of the LIBS plasma to chemical and physical prop-
55 erties of the sample, also known as matrix effects, as well as to experimental
56 parameters and conditions [19, 20, 8]. In particular for the complex geologi-

cal samples, this results typically in a low reproducibility of LIBS data which can then affect the accuracy of calibration models used for predicting elemental abundances [25]. Besides analytical approaches for reducing the influence of matrix effects, statistical methods such as principal component analysis (PCA) and partial least squares regression (PLS-R) are standard methods in LIBS data analysis [26].

For this study, LIBS data was collected during an interdisciplinary summer school held on Vulcano (Eolian Islands, Italy) in June 2019. The summer school focused on the robotic exploration of extreme environments ranging from the deep sea to planetary analogues. Vulcano offers a broad range of volcanic terrains, morphology and rock types for such planetary analog studies [27]. The geological evolution of Vulcano commences from 127 ka to present days, with the last major eruptive phase occurring in 1890 [27]. A number of eruptive episodes developed the present day morphology of the island, consisting of two intersecting caldera in the southern and central part of the island, and a smaller, more recent cone complex to the North, called Vulcanello. On Vulcano, a broad chemical variability of igneous products can be found, ranging from basalt to rhyolite, and including particularly alkaline products such as shoshonite and trachyte [28]. Hence, Vulcano is an ideal site to test new instruments and methods for geochemical investigation as it is possible to analyze a broad range of volcanic deposits, both in chemistry and physical properties. Different sites on the island were not only investigated with LIBS but also with other spectroscopic instruments such as a visible and near infrared spectro-radiometer and a portable Raman spectrometer. The three spectroscopic methods are of high interest for planetary in-situ explo-

82 ration by mobile spacecrafts. A combined analysis of the data from all three
83 spectroscopic techniques is planned and first results can be found in [29, 30].
84 Besides the spectroscopic analysis, further experiments were conducted with
85 the general objective of the summer school to learn about robotic exploration
86 for space and deep sea research. Regarding the robotic in-situ exploration of
87 planets and other bodies in the Solar System, the island offers the possibility
88 to study various planetary analogous sites with igneous minerals in volcanic
89 ashes, glasses or just lava flows that might be found similarly on other bodies
90 showing volcanism in the Solar System [31]. Evaluating the performance, ap-
91 plicability, and potential of the different spectroscopic methods at this place
92 has therefore a high relevance and can provide input for present and future
93 robotic space exploration missions.

94 For the LIBS measurements, a commercial handheld LIBS instrument
95 was used (details in Section 2). In recent studies, the same type of instru-
96 ment was used to analyze collected geological samples in laboratories where
97 promising outcomes for mineral identification and elemental quantification
98 were reported relying on statistical as well as on analytical approaches [32–
99 36]. One group also reported first tests from a volcanic field-site in New
100 Mexico, USA [37]. A recent review gives an overview of the growing product
101 range of handheld LIBS instruments and studies using these [38]. Most pre-
102 sented studies focus on the evaluation of quantification accuracies on samples
103 measured in a laboratory setting which is a crucial factor for the performance
104 of LIBS instruments. However, in this work we evaluate the performance of
105 such a commercial handheld LIBS instrument directly in the field without the
106 purpose of reporting quantitative results. We analyzed the natural surface in

107 its original environment, which poses additional challenges compared to mea-
108 surements in the laboratory. Experimental parameters such as the sampling
109 distance and the angle of incidence of the laser can be fixed in laboratory
110 measurements which usually improves the performance of LIBS measure-
111 ments. Moreover, while it is an advantage of LIBS that sample preparation
112 is not necessarily needed, samples with, for example, ideally flat surfaces can
113 be prepared for laboratory LIBS investigations for improved LIBS measure-
114 ments [22]. In the field, however, ideal positioning of the used handheld LIBS
115 instrument is not always possible and affects the collected data.

116 The focus of this study is to analyze the performance of a commercial
117 handheld LIBS device in a field setting and to identify the associated chal-
118 lenges compared with laboratory studies. We first present methods to vali-
119 date our approach using a laboratory study simulating varying distances be-
120 tween the instrument and sample. We then discuss our LIBS data acquired
121 at a field site on the island Vulcano characterised by layered volcanic ash. A
122 PCA analysis was then performed on this dataset as a first data exploration
123 method followed by a detailed layer-by-layer investigation of the observed
124 elemental emission line intensities with respect to the expected mineralogy
125 of the outcrop. Even though the LIBS spectral characteristics depend on
126 the specific experimental parameters and local ambient conditions, our re-
127 sults provide general and practical considerations for both terrestrial and
128 extraterrestrial applications such as by robotic platforms or for human in-
129 situ exploration of the Moon [39], where astronauts could be equipped with a
130 handheld LIBS instrument to analyze the geochemical composition of lunar
131 rocks and regolith.

132 2. Instrumentation and method

133 2.1. LIBS handheld device and method

134 For the field measurements, a commercial portable handheld LIBS instru-
135 ment, namely a Sci-Aps Z-300, was used. The instrument uses a Nd:YAG
136 laser operated at its fundamental wavelength of 1064 nm with a repetition
137 rate of 10 Hz and a laser energy of 5-6 mJ per pulse. The focused laser beam
138 size is in the order of 50 μm . A wide spectral range of 190-950 nm is cov-
139 ered by three spectrometers which are equipped with charge-coupled devices
140 (CCD). A detailed description of the predecessor model Z-500 can be found
141 in [32]. The difference lies only in the smaller spectral range of the Z-300,
142 as compared to the Z-500. The wavelength calibration is done internally by
143 the instrument by pointing the laser to a metal plate inside the instrument
144 when the instrument is switched on. This calibration needs to be repeated
145 after a fixed time interval which was set to 30 min in our case, to account for
146 changing conditions such as the instrument's inner temperature. The volume
147 in which the LIBS plasma evolves is kept under a constant Ar flow of 12 psi
148 during the measurement because emission line intensities are usually stronger
149 in Ar atmosphere than in ambient (terrestrial) conditions [40, 41]. The LIBS
150 plasma, and therefore its emission characteristics, depend on the atmospheric
151 pressure and gas composition where physical properties of the gases such as
152 the ionization energy and the heat capacity are important factors [42]. This
153 is a critical aspect to consider when planning a LIBS instrument for planetary
154 exploration as other planetary bodies have different atmospheric conditions
155 from Earth, resulting in different LIBS plasma characteristics [16]. With
156 regards to Ar, its physical properties are beneficial for LIBS analysis com-

157 pared to terrestrial conditions as discussed in detail by [40]. Furthermore,
158 the LIBS plasma in Ar atmosphere has a nearly uniform distribution of tem-
159 perature and electron density which reduces the effect of self-absorption and
160 emission line shifts [43]. However, it is important to point out that the use
161 of Ar results in the emission lines of Ar appearing in the LIBS spectra. At-
162 mospheric emission lines are common in LIBS data obtained in non-vacuum
163 conditions as species from the atmosphere contribute to the plasma, such as
164 carbon emission from a Martian atmosphere [44], or nitrogen in LIBS spectra
165 obtained in terrestrial conditions.

166 A single measurement with the handheld LIBS instrument consists of a
167 raster with multiple ablation points. For this field study and the laboratory
168 study (see Section 2.3), a 3×4 raster was selected in which the distance
169 between the outer borders of individual craters is $\approx 40 \mu\text{m}$. At each point,
170 five successive laser pulses are done, but only the radiation from the last three
171 induced plasmas is recorded. The first two laser pulses are called "cleaning
172 shots" as the shock-wave of the LIBS plasma removes dust or superficial
173 contamination from the sample and thin layers (e.g. from weathering) are
174 ablated. The detector measures the radiation from each plasma starting after
175 a delay of 630 ns after the laser pulse and during an integration time of 1 ms.
176 The described settings of timing, size of the raster, and number of laser pulses
177 can be changed, however, we measured all samples with the same settings
178 for a better comparability. The measured spectra of each individual point in
179 the raster, except for the cleaning shots, is accumulated and from the whole
180 raster, an average spectrum is obtained.

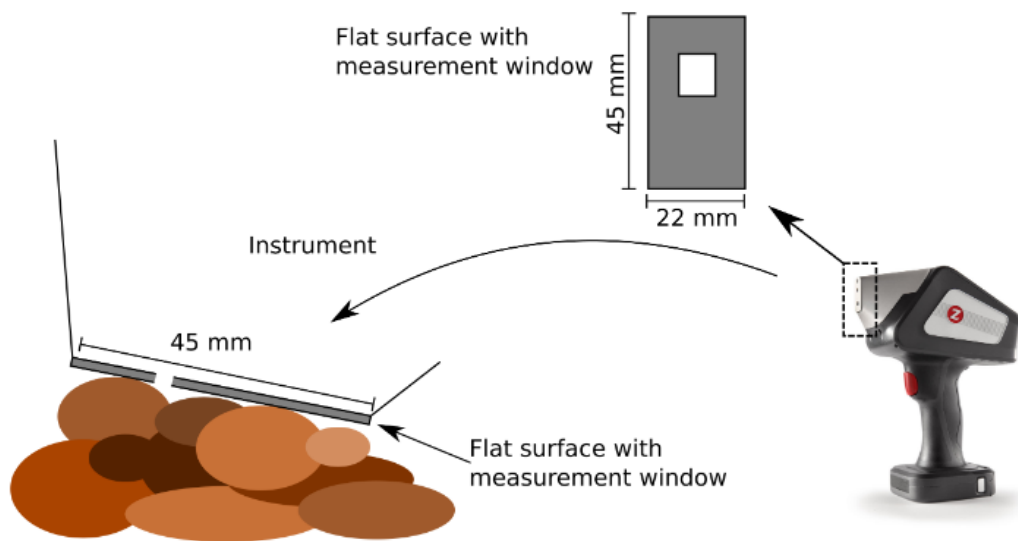


Figure 1: Illustration of one of the major challenges for LIBS field measurements with the handheld device: surfaces that are not flat on the scale of the instrument's contact flat surface ($45 \times 22 \text{ mm}^2$) can not be measured with a direct contact between the instrument and the sample. As a consequence, the distances can vary in the range of a few centimeters.

181 2.2. Application in the field

182 As the measurements were performed in the field it was not possible to
183 keep the experimental conditions as constant and ideal as in a controlled ex-
184 periment in the laboratory. The experimental parameters that were changing
185 the most in the field were the instrument distance to the sample, the angle of
186 incidence of the laser radiation on the naturally rough surfaces and the angle
187 under which the plasma radiation is collected. The analysis window of the
188 instrument is located in a flat surface with an area of size $2.2 \times 4.5 \text{ cm}^2$ which
189 should be placed in contact to the ideally flat sample surface for optimal data
190 acquisition. If the contact between the instrument and the sample's surface
191 is not well accomplished, the sampling area might not be in the best focus
192 position for the most effective material ablation. This was frequently the
193 case for the samples analyzed in the field and a sketch illustrating this situa-
194 tion is shown in Figure 1. The encountered natural surfaces on Vulcano were
195 often rough on scales much smaller than the flat area of the instrument and
196 therefore challenging to measure with the handheld LIBS device. This led to
197 LIBS spectra acquired with varying distances [on the scale of millimeters up](#)
198 [to a few centimeters between the sample surface and the instrument](#). Related
199 to variations in the sampling distance is the contribution of Ar atoms to the
200 LIBS plasma from the introduced Ar atmosphere as it can change depending
201 on where the breakdown takes place. Another experimental parameter that
202 was changing in the field was the surrounding temperature [which does not](#)
203 [affect the LIBS plasma itself but can slightly change](#) the detection geometry
204 and therefore the wavelength calibration. Consequently, recalibration of the
205 wavelength was done regularly.

206 During the data analysis some spectra showed strong emission lines of
207 Ar and contain almost no signals from other elements. The presence of Ar
208 emissions in the spectra was expected but not the relatively strong impact
209 on the spectra quality. In such cases, it is most likely that the distance to
210 the sample was too large to create the LIBS plasma on the surface of the
211 sample and the breakdown was almost completely in the Ar atmosphere.
212 These spectra provide no relevant information about the geochemistry of
213 the investigated samples and were therefore rejected from further analysis.
214 An example of such a spectrum is shown in Figure 2 (*top*) where strong Ar
215 emission lines in the spectral range above 650 nm (marked with dashed line)
216 can be seen. During the measurement campaign, it was difficult to control the
217 exact distance to the sample and hence the quality of the LIBS spectra. An
218 automated procedure to identify and remove these primarily Ar spectra was
219 applied after data collection. The procedure relies on summing the counts in
220 the spectral ranges below and above 650 nm, respectively. All Ar emission
221 lines are in the spectral range above 650 nm and if the ratio of the summed
222 counts above and below is larger than one, the spectrum was rejected. With
223 this approach, $\approx 14\%$ of the spectra, 8 out of 57 spectra, were rejected.
224 An example for a spectrum which was not rejected and contains relevant
225 geochemical information is shown in Figure 2 (*bottom*).

226 2.3. Laboratory study: effect of varying distance

227 As the distance of the instrument to the sample was found to strongly in-
228 fluence the quality of the LIBS data, a laboratory experiment was performed
229 to investigate how this affects in particular the Ar emission. A gypsum
230 ($\text{CaSO}_4 \times 2 \text{H}_2\text{O}$) pellet was chosen as the target sample for its homogeneity

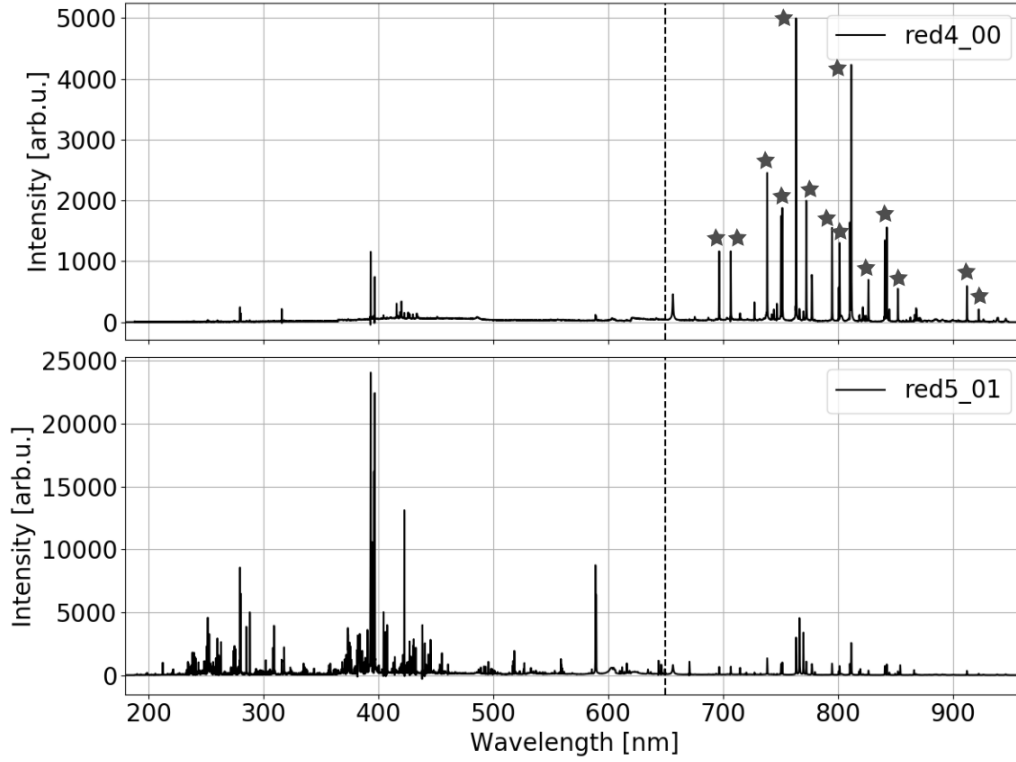


Figure 2: *Top*: Example of a spectrum with strong Ar emission lines (marked with stars) and with almost no other information. The total intensity of this spectrum is dominated by emission lines above 650 nm (dashed line). The ratio of the integrated intensities above and below 650 nm is larger than one and the spectrum was rejected from further analysis. *Bottom*: Example of a good quality spectrum with stronger emission lines in the spectral range below 650 nm than above this wavelength. This spectrum contains information about the elemental composition of the target and has a ratio of integrated intensities above and below 650 nm smaller than one.

231 and simple sample matrix structure. This allows to relate changes in the Ar
232 emission mainly to the change in distance and reasons the choice of sam-
233 ple which is not motivated by expected minerals at the measurement site
234 in the field. For the experiment, the instrument was fixed and the sample
235 was mounted on a stage. The height of the stage was changed from a posi-
236 tion where the instrument and the sample were in direct contact to a position
237 where the distance was ≈ 40 mm. At five different intermediate positions, five
238 measurements were performed, respectively. Several neutral and one ionic Ca
239 emission lines were chosen for the analysis. All Ar emission lines in the data
240 were identified to come from only neutral Ar. Two moderately intense and
241 free standing Ar lines, one close to 700 nm and one Ar line near the end of the
242 spectral range beyond 900 nm were selected for analysis. All emission lines
243 were fitted with Lorentzian line shapes in each of the five spectra per position
244 and the intensities were averaged. In Figure 3, the intensities of the Ar and
245 Ca emission lines are shown for increasing distance between the sample and
246 the instrument, and different trends of the Ca and the Ar emission lines can
247 be observed. The emission lines of Ca(I) and Ca(II), which come from the
248 sample matrix, are overall decreasing with increasing distances. However,
249 the Ca (I) emission lines show a small increase from 0 mm distance to 10 mm
250 distance, which is not observable for the Ca (II) emission line. Furthermore,
251 the Ca (II) drops more strongly than the Ca (I) intensities after the distance
252 of 20 mm. This indicates that the plasmas at larger distances have lower
253 temperatures since ionized species are more abundantly present and excited
254 in high temperature plasmas. In contrast to the Ca emissions, the intensities
255 of Ar atoms emission lines show an increase until a distance of 20 mm and

256 then decrease for larger distances. This suggests that a distance of 20 mm
257 to the sample is optimal for Ar emission, while the emission of components
258 coming from the sample is reduced.

259 When comparing the ratio of the integrated intensities above and below
260 650 nm, as was also done for the field data, the ratio is only larger than
261 or close to one for the instrument-sample distance of 40 mm. However, the
262 spectra at this distance are already of a bad quality and the reason for the
263 comparatively small ratio can be found in the characteristics of the LIBS
264 spectrum of the gypsum sample. Gypsum has a large concentration of Ca
265 (≈ 23 wt %) which is most likely larger than in the ash layers measured on
266 Vulcano. Furthermore, Ca lines tend to be strong already at small concen-
267 trations which is not the case for most other elements. With the gypsum
268 sample, the integrated intensity below 650 nm is larger than it would be for
269 samples with lower Ca abundances. Additionally, the emissions of Ca as well
270 as O above 650 nm contribute to the sum of the range with the Ar emission
271 lines. Thus, with such samples, the ratio at which a spectrum should be
272 rejected should be chosen to be much smaller. With a threshold ratio of 0.4,
273 all spectra measured at 40 mm distance, and almost all at 30 mm, would be
274 rejected with the discussed approach.

275 This laboratory study further shows that the Ar emission is not suited to
276 compensate for effects of varying sampling distances as the emissions coming
277 from elements in the sample (here: Ca) and the Ar emissions behave in
278 different ways. Similar results regarding the contribution of C emission from
279 a simulated martian atmosphere to LIBS plasmas were shown in [44] for other
280 varying experimental conditions, such as varying laser irradiance or varying

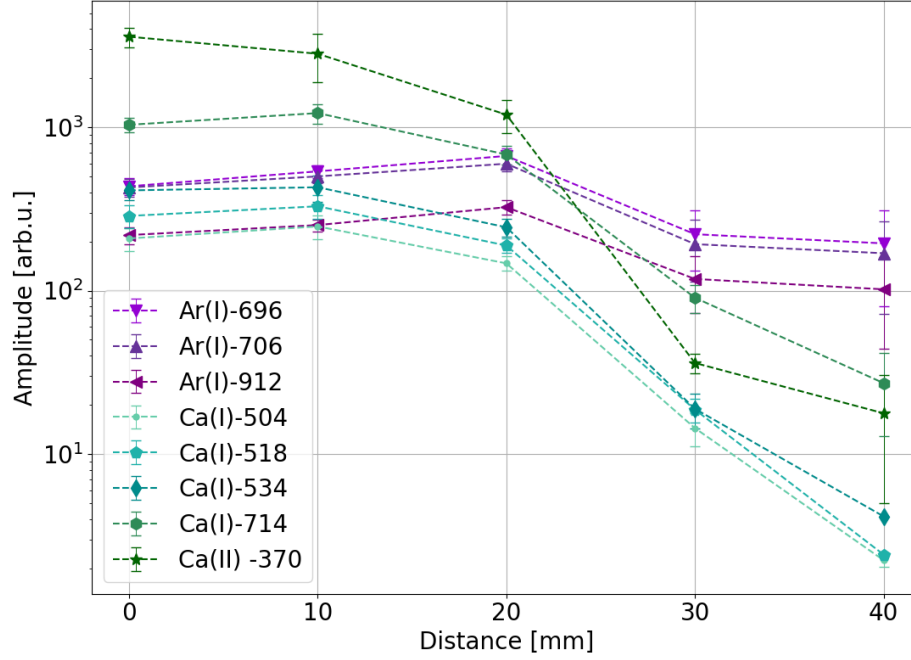


Figure 3: Fitted intensities of Ar and Ca emission lines for increasing distances between the sample and the instrument. The error bars indicate the standard deviation of five measurements. The Ar emissions coming from the atmosphere show a slight increase followed by a decrease while the Ca emissions decrease only with increasing distance.

281 grain sizes.

282 2.4. Data pre-processing

283 Prior to the actual data analysis, LIBS data needs to be pre-processed [25]
 284 and particularly for the spectra in this study, which were measured at vary-
 285 ing distances, a dedicated data treatment is essential. Different approaches
 286 for data normalization were tested and evaluated. In the literature, it is sug-
 287 gested that normalization to Ar emission lines contributing from the atmo-
 288 sphere can improve univariate calibration curves [41]. Our laboratory study

with varying sampling distances (Section 2.3) showed, however, that the Ar emissions are not suitable for normalization of our data. Despite having rejected the spectra with the strongest Ar contributions, when normalizing to the total emission intensity the PCA outcomes were strongly influenced by the Ar emissions, which was observed in the PCA loadings. Variance in the data due to the elements of the samples remained mostly hidden with this approach. A similar result was obtained when normalizing to the maximum intensity of the spectrum. In order to avoid this strong influence of the non-analytical Ar emission lines on the PCA, they were masked in the spectra. All Ar emission lines in the present spectral range were thus replaced by the average of the two values at the borders of the corresponding emission line ranges. A list of all masked Ar emission lines can be found in Table 1. This approach seemed most suitable for our objective to study the geochemical variations and elemental trends in the ash layers with PCA. After all observed Ar emission lines were masked, the integrated emission intensity of each spectrum was used for normalization. In a further step the spectra were mean centered and divided by their standard deviation before PCA so that all spectra have a mean value of zero and a standard deviation of one.

3. Investigation of volcanic deposits - description and LIBS results

3.1. Description of the outcrop

The island of Vulcano (Aeolian Islands, Sicily Italy) consists of several volcanic edifices whose formation overlapped in time and space ([27] and references therein). One of the most recent areas of volcanic activity is the northern peninsula Vulcanello composed of a basal lava platform (1.9 ka) super-

Table 1: Ar(I) emission lines as listed in the NIST database [45] that were masked in the spectra in order to suppress their influence on the analysis. Also shown are the ranges in which values were replaced by the average of the two values at the end and the beginning of the range.

λ (NIST) [nm]	masked range [nm]
696.5	695.6 - 697.5
706.7	705.7 - 707.7
727.3	726.0 - 728.5
738.4	737.3 - 739.6
750.4; 751.5	749.4 - 752.7
763.5	762.1 - 764.9
772.4; 772.4	771.5 - 773.3
794.8	793.8 - 795.8
800.6; 801.5	798.6 - 803.6
810.4; 811.5	808.9 - 813.4
826.5	825.6 - 827.4
841.8; 842.5	839.9 - 843.7
852.1	851.3 - 852.9
912.3	911.4 - 913.3
922.5	921.7 - 923.1

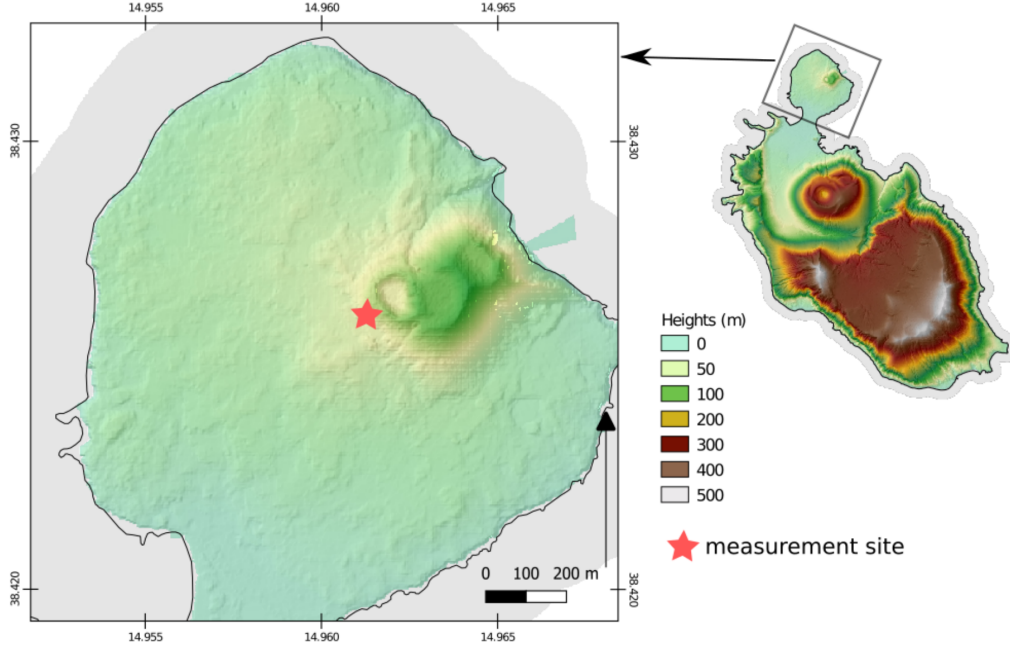


Figure 4: Map of Vulcano showing a detailed inset of the northern peninsula and Vulcanello. The star symbol marks the outcrop location of this study.

313 imposed by three partially overlapping scoria cones (0.4 ka) aligned NE–SW
 314 along the northern ring fault of the La Fossa caldera [27]. An overview map
 315 of Vulcano with a detailed view of Vulcanello is shown in Figure 4. Vulcanello
 316 mostly erupted alkali-rich shoshonitic products with a few latitic products
 317 characterizing the last cycle of activity [46]. The outcrop investigated in this
 318 study is located at the foot of the southernmost cone, which is considered
 319 to be the youngest and is dominated by pyroclastic deposits [27]. These are
 320 composed of a several meters thick thinly bedded, vesiculated and multi-
 321 colored ashes and lapilli of the vu3_b member of the Vulcanello formation [47].
 322 A detailed image of the outcrop is shown in Figure 5 (*a*).

323 As described in Section 2, one LIBS measurement in this study consists of

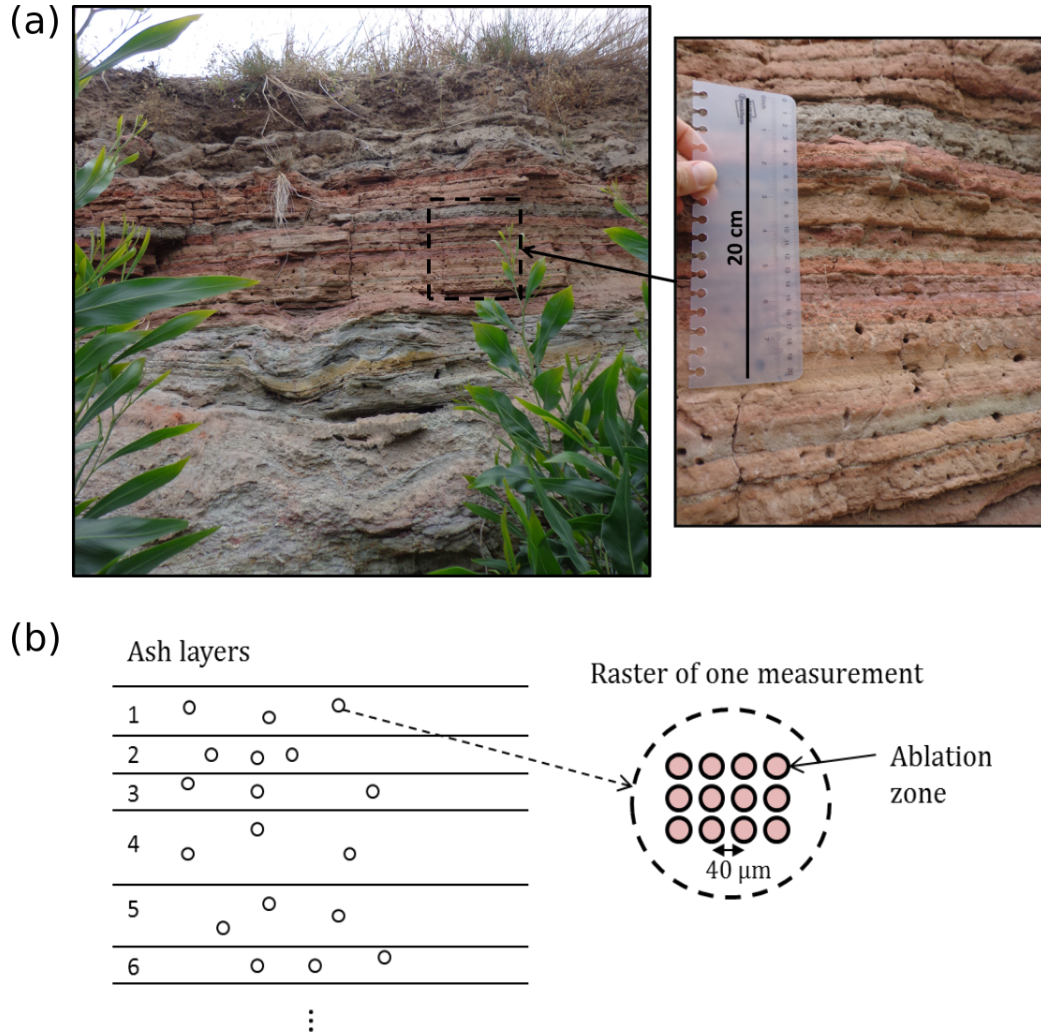


Figure 5: (a) Image showing the investigated outcrop on Vulcanello with layers of differently colored volcanic ashes. The dashed black box marks the area that can be seen in the zoom *right*. The layers not only differ in color, some of them are hard rocky surfaces while the majority consists of loose, poorly consolidated material. (b) Schematic drawing of measurement procedure. In each layer, three different locations were measured while at each position material was ablated in a raster of 3×4 positions.

324 a raster with 12 ablation zones in total. A schematic drawing of the measure-
 325 ment procedure for the investigated ash layers can be seen in Figure 5 (b). In
 326 each layer, three LIBS measurements were acquired and in total, 19 layers
 327 were investigated of which the uppermost layers can be seen in the zoom
 328 in Figure 5 (a). For a better traceability, we assigned numbers to the layers
 329 from top to bottom along with a color code of "gray", "red", "orange", or
 330 "yellow" based on our visual inspection. Repeated colors were numbered as
 331 well. A list of the labeled layers is provided in Table 2 and can be used for
 332 comparison with the image of the outcrop in Figure 5 (a). Not only the colors
 333 of the layers change but also their physical appearance as some layers appear
 334 harder while others are more brittle and less robust in comparison, and some
 335 even crumbled during the measurement. This is an additional aspect that
 336 needs to be considered in the LIBS analysis since the quality of a spectrum is
 337 influenced by the laser-matter interaction and how well the laser couples to
 338 the sample mainly depends on the physical matrix of the sample. In general,
 339 harder and more consolidated materials produce better LIBS spectra while
 340 loose materials and even soils are more difficult to analyze with LIBS.

341 3.2. LIBS spectra

342 For a first overview of the data, the average and in some cases single LIBS
 343 spectra are shown for each layer in Figure 6. The spectra are presented in
 344 the order of the layers from top to bottom and their colors correspond to the
 345 assigned layer color. In these spectra, the Ar emission lines were not masked
 346 as described in Section 2.4 to emphasize that they are present in all spectra
 347 with variable intensities. For each layer, n gives the number of spectra and
 348 some intervals with strong emission lines of Si, Mg, Al, Ca, Fe, Na, CaF, H,

Table 2: Naming of the layers from top to bottom. The first (top) layer is layer 1 and has the name gray 1 while the last (bottom) measured layer is gray 6.

Layer	Naming	Layer	Naming
1	gray 1	11	yellow 2
2	red 1	12	orange 3
3	orange 1	13	gray 4
4	gray 2	14	orange 4
5	yellow 1	15	orange 5
6	red 2	16	red 5
7	gray 3	17	gray 5
8	red 3	18	yellow 3
9	red 4	19	gray 6
10	orange 2		

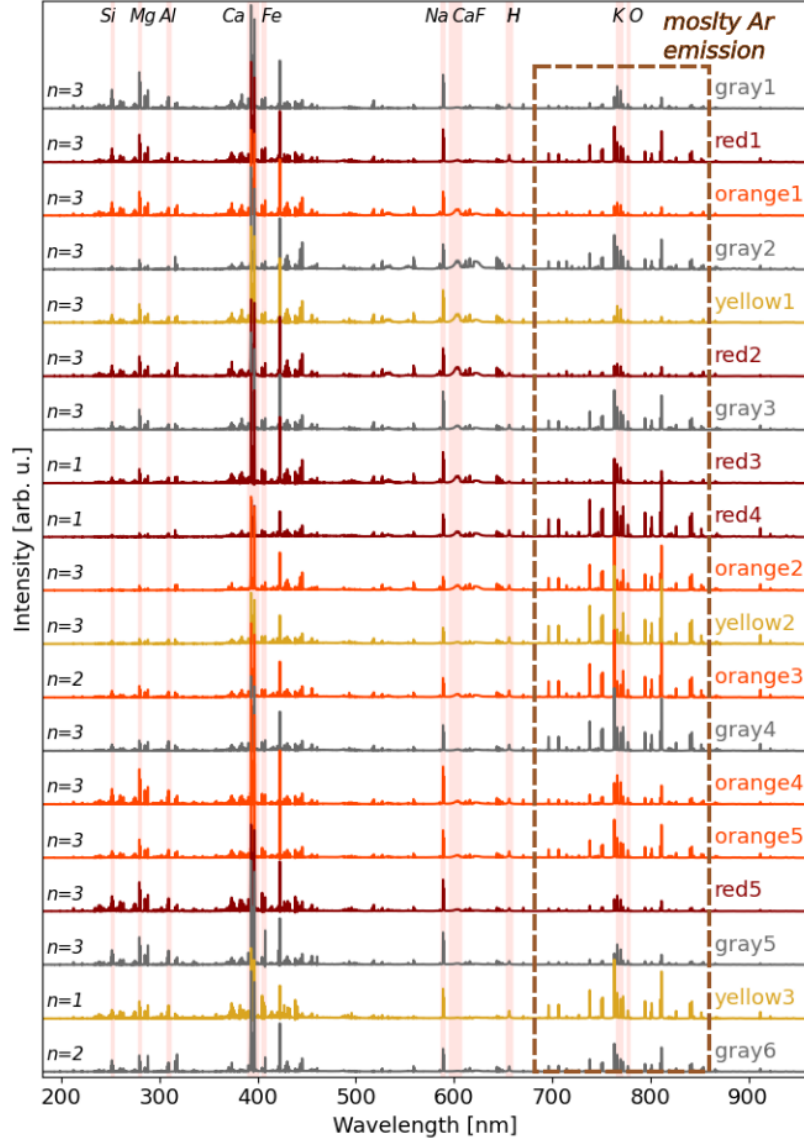


Figure 6: Mean spectra or single spectrum of each layer in the order from top to bottom to be compared with Figure 5. Here, the spectra were normalized by their total emission intensity but the Ar emission lines in the spectral range > 650 nm were not masked in order to visualize their influence. For each layer n indicates the number of available spectra that were averaged if $n > 1$. Spectral ranges of Si, Mg, Al, Ca, Fe, Na, CaF, H, K, and O emissions are marked in light red.

349 K, and O were marked in light red but clearly each spectrum contains more
350 emission lines which could not all be marked in this representation.

351 3.3. Data exploration - PCA

352 In order to explore the data and to investigate chemical variations of
353 the different ash layers, a PCA was performed with the LIBS spectra that
354 fulfilled our quality criterion. In Figure 7, the PC 1/PC 2, PC 3/PC 4, and
355 PC 5/PC 6 score plots are shown. For each PC, the explained variance in
356 the data by the particular PC is given in brackets. The accumulated sum of
357 the explained variance up to PC 6 is 89.9 %. This indicates that the variance
358 in the dataset is distributed over multiple spectral features, as 10 PCs (not
359 shown here) are needed to explain more than 95 % of variance in the data.
360 Furthermore, for interpretation and discussion of the PCA, the loadings of
361 PC 1-6 are given in Figure 8. The loadings indicate correlations between the
362 PCs and spectral features, and thus how large the influence of these spectral
363 features on the particular PC is.

364 In general, regarding the score plots in Figure 7, where the score value of
365 a spectrum is colored by the color of the corresponding layer obtained from
366 visual inspection, no clustering or trend due to the layer color is observable.
367 However, colors ascribed to the layers are qualitatively and subjective. For
368 individual layers, which are represented by symbols in the score plots (Fig-
369 ure 7), similar trends for all spectra from the same layer can be seen in some
370 cases. For example, the scores of layer *red5* are relatively close to each other
371 in all three score plots. Furthermore, there are also cases where the scores of
372 two spectra from one layer are very similar and plot close together while the
373 third one has score values rather different from the others and plots further

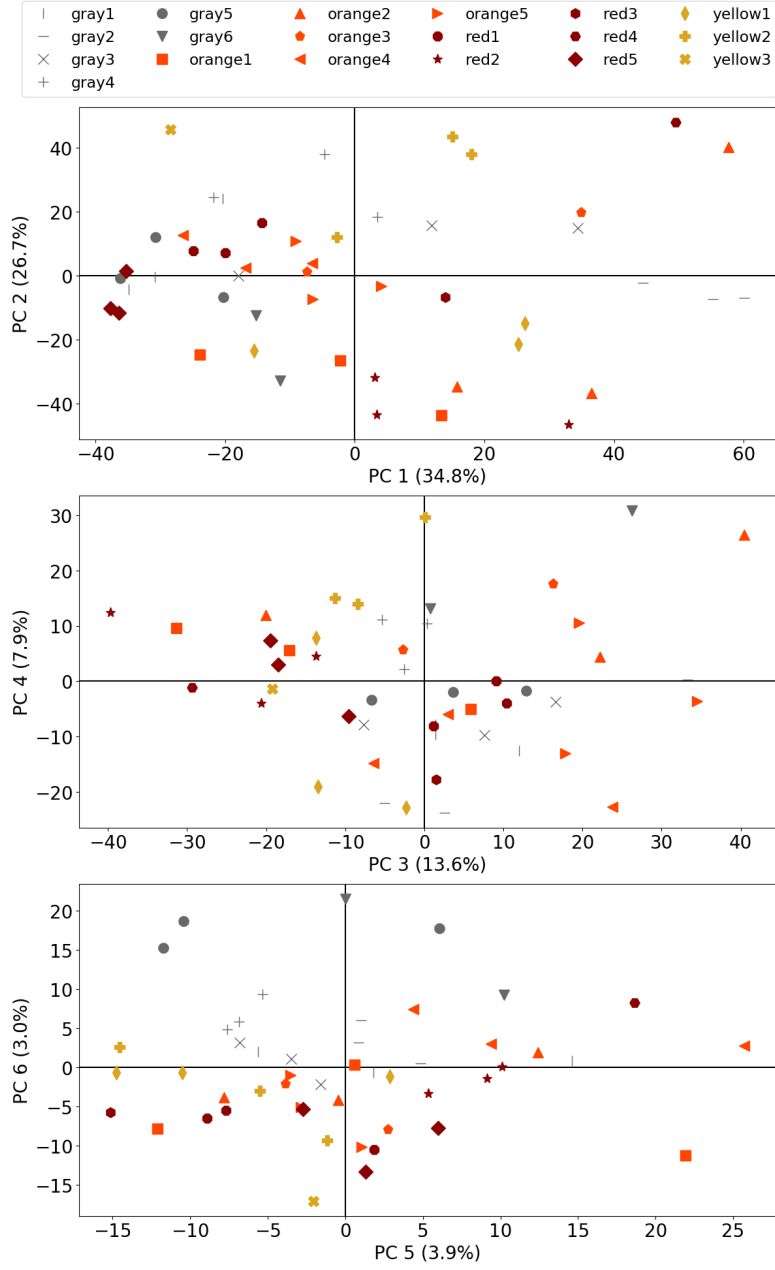


Figure 7: Score plots of PC1/PC2, PC3/PC4, and PC5/PC6 where the number in brackets is the explained variance of the dataset by each component. The colors correspond to the color of the layer attributed from visual inspection while the symbol indicates individual layers. There is no distinct grouping according to layer color observable, but for some individual layers consistent trends for spectra from the same layer can be seen.

374 away, see for example the scores of layer *yellow1*. In general, these trends
375 are promising as they allow to observe elemental variations among the layers
376 and to evaluate the homogeneity of the layers as well as the reproducibility of
377 the measurements. Larger distances between score values of spectra from the
378 same layer can serve as an indication for the two latter mentioned factors.
379 However, besides the occasionally observable trends, a clear clustering due to
380 the individual layers is not observable. One reason for this can be the already
381 discussed not well controllable distance between the sample and the instru-
382 ment which introduces variations among the spectra of one layer. To reduce
383 those experimental influences as seen in this analysis and to increase high
384 quality data per layer it would be worthwhile to analyze more positions per
385 layer in future geochemical field investigations with such a handheld LIBS
386 device. In the following, we discuss briefly the observations from the PCA
387 to reveal correlations and give interpretations on the score values and the
388 loadings.

389 First, the loadings of PC 1 mainly distinguish between spectra with rather
390 strong emission signals of Ca, K, and O as well as molecular emission bands
391 of CaF and spectra with relatively strong emission lines of Al, Si, Mg, and
392 Na. Molecular emission bands, as those of CaF, can serve as an indirect
393 detection of elements which are otherwise challenging to detect in the used
394 spectral range (200-900 nm) such as Cl and F [48–50]. For the Ca emission
395 lines, the neutral and single ionized lines behave differently. The neutral Ca
396 emission lines emit in a spectral range larger than 400 nm and have positive
397 correlations with PC 1. On the other hand, the ionized Ca emission lines
398 are in the spectral range below 400 nm and show only small correlations

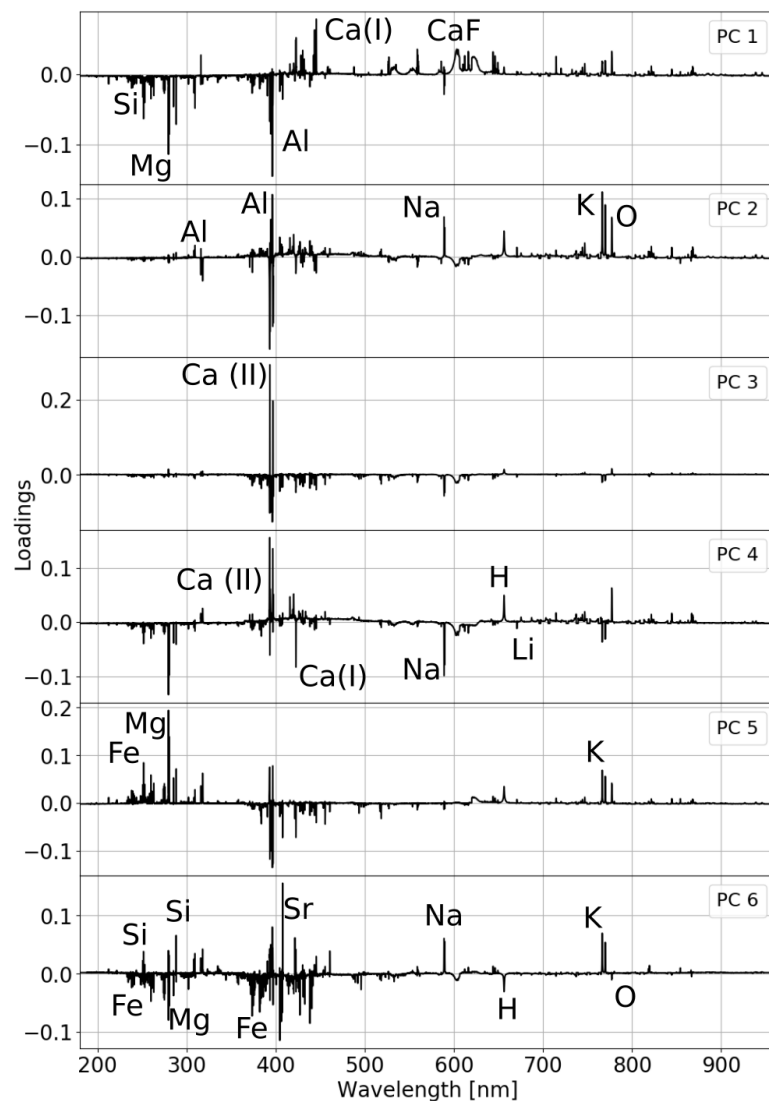


Figure 8: Loadings of PC1-PC6. Positive values indicate a positive correlation with the PCs resulting in positive score values of spectra which have features at these particular positions. For negative loadings the opposite applies. For clarity, annotations of the elements were not done for each PC. For some Ca features, the ionization state was given as anti-correlations of neutral and first ionized Ca emissions were observed.

399 with PC 1 that are overall negative, except for the Ca (II) line at 315.9 nm.
 400 One reason for this difference could be changing plasma conditions, such as
 401 different plasma temperatures and electron densities that favor either neutral
 402 or ionized Ca emission. But also the varying distance could be responsible as
 403 slightly different trends with distance were observed for neutral and ionized
 404 Ca emission lines in the laboratory study discussed in Section 2.3. A zoom of
 405 the loadings of the 6 PCs to the spectral range 390-400 nm where two Al (I)
 406 and two Ca (II) can be found is shown in Figure 9. The dashed lines mark the
 407 expected center positions of the emission lines and differences in the emission
 408 line shapes and positions are observable for all PCs. These changes could
 409 be caused by self-absorption or line shifts. Self-absorption is an effect where
 410 highly abundant elements emit photons in the hot plasma core which are
 411 reabsorbed by atoms of the same element in the colder outer plasma regions.
 412 This can lead to more broadened emission lines and even dips in the center of
 413 emission lines [19, 7]. Line shifts can occur because of different surrounding
 414 pressure conditions [51] but also because of instrumental factors such as
 415 the collection angle (sub-optimal positioning of the instrument can lead to
 416 aberrations) or the repeated wavelength calibration that was necessary due
 417 to the heat. For PC 1 the observed shapes of the Ca (II) emission lines are
 418 most likely a result of different degrees of self-absorption. Stronger self-
 419 absorbed lines have more extended wings which show a negative correlation
 420 with PC 1. To conclude, it is challenging in particular for the Ca (II) emission
 421 to derive interpretations related to abundances in the layers as these lines
 422 show influences of plasma as well as instrumental conditions.

423 PC 2 has the largest positive correlations with Al, Na, H, K, and O emis-

424 sion lines, which can indicate the presence of alkali-rich feldspars in layers
425 which high score values on factor 2. On the other hand, negative correlations
426 are mainly observed for Ca emissions, neutrals and first ionized ones.

427 PC 3 shows the strongest positive correlation with the usually strongest
428 Ca (II) emission lines at 393.4 nm and 396.8 nm, see Figure 9. Narrow Ca (II)
429 lines have a positive correlation while broader, most likely self-absorbed,
430 emission lines have a negative correlation with PC 3. Other positive corre-
431 lations are observed for H and O emission lines but much smaller than the
432 narrow Ca (II) emission lines.

433 PC 4 reveals a strong influence of Mg, Na, and Ca (I) emission lines re-
434 sulting in negative score values for spectra that exhibit these features. On
435 the other hand, stronger H and O features lead to positive score values on
436 PC 4. Ca (II) emission lines reveal an influence of the line position of the two
437 strongest ones on PC 4, see Figure 9.

438 PC 5 mainly separates spectra with somewhat stronger emission lines of
439 Fe, Si, Mg, and K from those with Ca features. For this PC, a further
440 inconsistent observation can be made for neutral Al emission lines, as the
441 lines at 308.2 nm and 309.3 nm have a positive correlation with PC 5 while
442 the ones at 394.4 nm and 396.2 nm have a negative one. This means, as
443 already seen for Ca emissions, that no relative quantitative conclusions from
444 PC 5 can be made for Al concentrations in the layers.

445 PC 6, finally, has positive correlations with emission lines of the alkalis
446 Na and K as well as with Si and is the first PC that shows clear Sr emission
447 lines. Negative correlations are observable mainly for Fe and Mg emissions.
448 Especially, the influence of Fe is higher on PC 6 than on all other previous

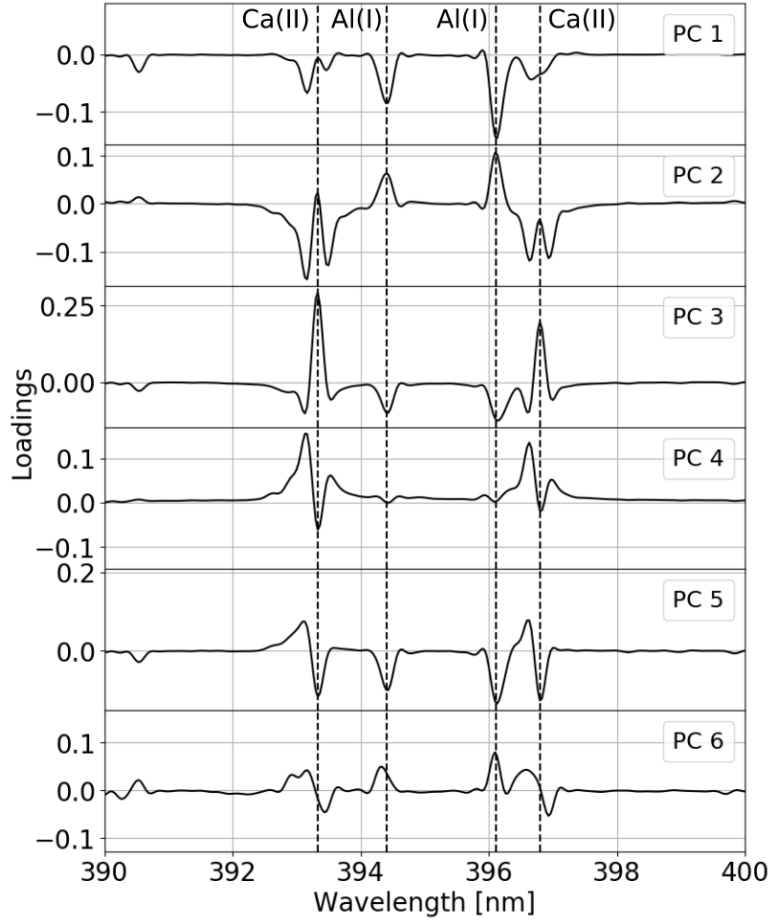


Figure 9: Same plot of the loadings as in Figure 8 but zoomed to the spectral range 390-400 nm in order to better visualize the different line shapes of the Ca (II) emission lines in the loadings. Line shapes that show not only changing peak heights but dips or zero crossings indicate that not only the intensity of the particular element has an influence on the PC. Effects that contribute to those line shapes can be, for example, shifts in the line position due to experimental conditions or self absorption of emission lines.

discussed PCs. The PC 5/PC 6 score plot in Figure 7, reveals the only but also slight trend due to color. Almost all spectra from layers considered as gray have positive score values on PC 6. Thus, red, orange, and yellow layers are expected to have higher Fe abundances than gray layers. The reason could be the presence of Fe-oxides which are responsible for reddish colors.

To summarize the observations from the PCA, clustering was observed for several individual layers but not between layers due to the color label. The results are promising as some trends according to individual layers became apparent. Furthermore, the loadings indicate influences of different elemental combinations and allow therefore to make relative predictions of elemental abundances from the spectra. Nevertheless, these predictions are challenging for elements whose emission lines show influences of line shape and line position in the loadings as observed mainly for Ca (II) in this analysis.

3.4. Layer-by-layer analysis

In addition to the PCA, a layer-by-layer analysis using univariate fits of several emission lines was done. Emission lines of major as well as minor and trace elements were fitted with Lorentzian curves. Besides the emission line fits, the intensity of the CaF molecular emission band was tracked by integrating the measured intensity in the interval 602-603.5 nm. For Ca, an emission line at 714 nm was selected which is less self-absorbed than the strong Ca (II) lines slightly below 400 nm. All results are shown in Figure 10 as single points which are at maximum three fits for one layer. The order from left to right in the plot corresponds to the order top to bottom of the outcrop. The dashed line connects the mean values of the shown fits. In some cases, the fits of one layer show a large scatter around the mean

474 value, but in other cases the fitted intensities are unambiguous, which is in
475 agreement with observations made in the PCA, see Section 3.3. The objective
476 of this analysis is to investigate elemental correlations among the layer and
477 possible depositional trends. Mostly major elements were discussed in the
478 PCA analysis while in this univariate approach minor elements that often
479 have only a few emission lines in the commonly used spectral range (200-
480 900 nm) can be included.

481 Similar to the PCA, no distinct trend of element abundances related to
482 color is observable. Nevertheless, except for the one spectrum of layer *red4*,
483 the red layers are relatively enriched in Fe whose oxides are responsible for
484 reddish colors. Regarding correlations between emission line intensities, a
485 distinct correlation between the Al (I) and the Si (I) emission lines is visi-
486 ble in Figure 10, which is confirmed by a high Pearson correlation coefficient
487 of 0.97 among the measurements. Such a correlation is characteristic of
488 products of volcanic origin. Additional but somewhat weaker correlations
489 are observable for the alkaline elements Na and K but also for Mg and Fe
490 which are typical elements of mafic rocks. The only clear anti-correlations
491 according to Pearson correlations are found for the Ca (I) emission line with
492 Al(I), Si (I), Fe(I), and Mg(I) line intensities. This is mostly in agreement
493 with the loadings of PC 1 discussed in the previous section as those indicate
494 an anti-correlation of Ca with almost all other elements, see upper plot in
495 Figure 8. In general, the observed correlations are in agreement with the
496 description of the ashes in [47]: The erupted lava is dominated by alkali rich
497 shoshonitic products which are igneous K-rich basaltic trachyandesites con-
498 taining alkali feldspars, olivines and pyroxene. Thus, the ashes are composed

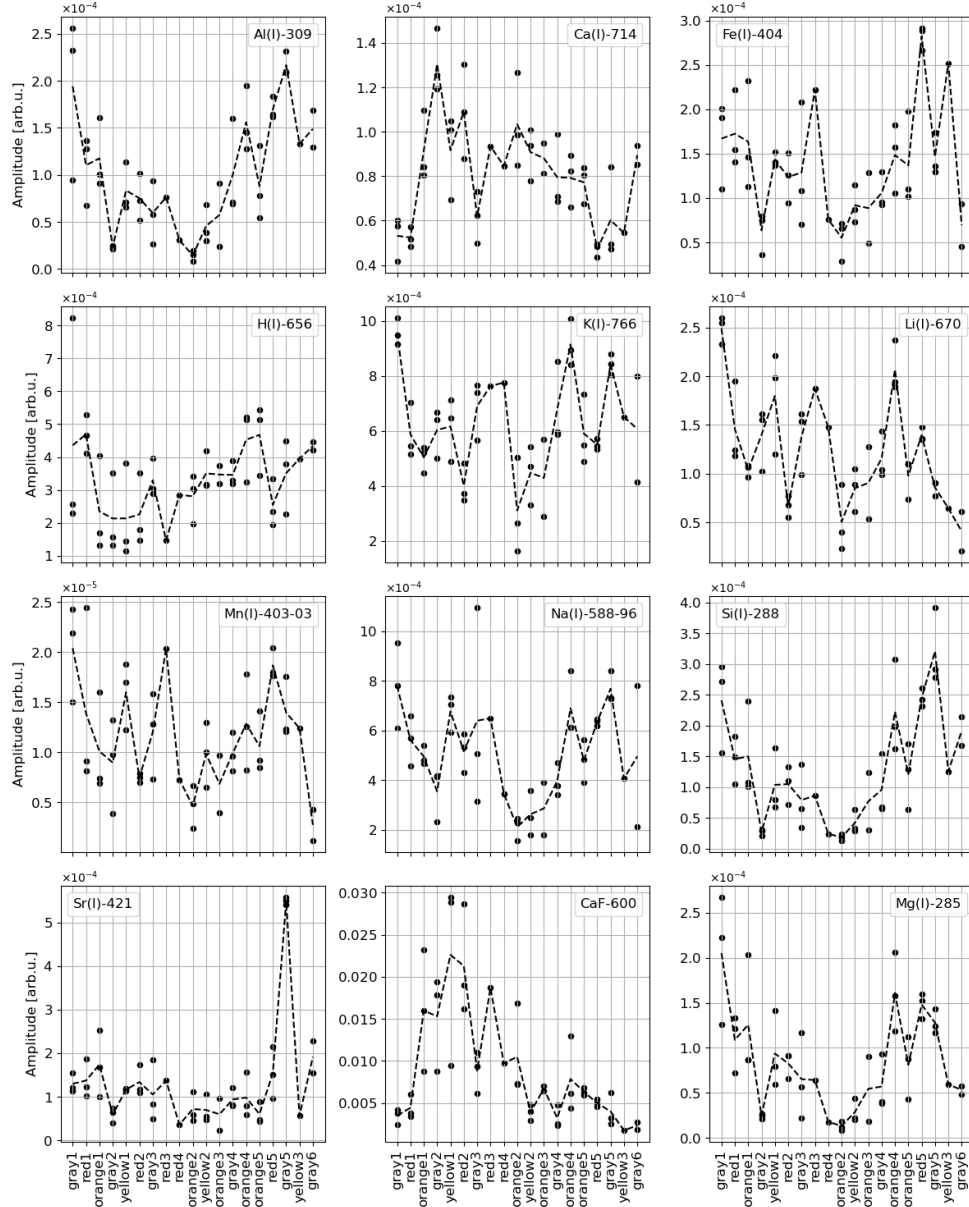


Figure 10: Emission lines of Al, Ca, Fe, H, K, Li, Mn, Na, Si, Sr, and Mg were fitted with Lorentzian curves and the results are shown here for the layers from top to bottom. The intensity of the CaF molecular band are integrated intensities in the range 602-603.5 nm. All results from the available spectra are shown while the dashed line connects the mean values of each layer.

499 of felsic and mafic minerals with high alkaline and low Ca contributions. Es-
500 pecially, the observed anti-correlation of Ca with all other elements confirms
501 the shoshonite-alkaline character of these igneous materials.

502 For the minor and trace elements, the strong Sr signal for layer *gray5*
503 in all three spectra is particularly noticeable. This observation can be com-
504 pared with the PCA in Section 3.3 as Sr emissions were identified to have
505 a positive correlation with PC 6. Indeed, all three spectra from layer *gray5*
506 have large positive score values on PC 6. Besides this strong Sr emission in
507 this layer, similar trends of the Sr emission line among the layers could be
508 identified with Al, Na, and Si emission lines. The Mn emission line has the
509 strongest correlation with the Fe emission line (Pearson correlation of 0.79)
510 which can be an indication for redox processes. But Mn has furthermore
511 positive correlations with the alkaline metals Li, Na, and K as well as with
512 Mg. Similar observations can be made for the Li emission line, which has
513 besides the correlation with the Mn emission, correlations with the lines of
514 K, Na, and Mg. The intensities of H and CaF are variable among the layers.
515 The H emission is known to be strongly influenced by matrix effects and
516 experimental conditions most likely due to its low atomic mass and behave
517 differently than heavier elements in the LIBS plasma [52, 44]. Thus, quan-
518 titative conclusions can only be made with care, especially with the rather
519 loose materials in this investigation. However, the lower part of the outcrop
520 seems to be overall more hydrated than the upper part. The CaF molec-
521 ular intensity cannot be related directly to F abundances [53] as the CaF
522 molecules form temporarily in the plasma and their concentration depends
523 also on Ca abundances. Nevertheless, the band intensity can be used for

estimates of the F concentration in the layers and a slight increase of the CaF signal after the second layer *red1* is observable followed by an decrease after layer *red4*. A similar trend can be seen for the score values on PC 1, which has the largest positive correlations with Ca (I) emission lines, indicating that there was enough Ca present in these layers in between to form CaF molecules in the LIBS plasma. Thus, these layers might have higher abundances of F containing minerals such as fluorite (CaF_2) or fluorapatite ($\text{Ca}_5\text{F}(\text{PO}_4)_3$). Indeed, the CaF band intensity is the only feature that has a positive Pearson correlation (0.65) with the Ca (I) emission line.

A distinct depositional trend is not observable in this layer-by-layer analysis, however, the igneous products associated with elements typical for felsic but also mafic minerals tend to be more abundant in the lower part of the outcrop. The middle part of the outcrop is dominated by Ca and F abundances while the upper part tend to contain again more felsic and mafic minerals.

4. Summary

During the measurements with the commercial handheld LIBS device in the field, it was not possible to bring the sample surface always in direct contact with the instrument due to a limited accessibility and naturally rough surfaces. Consequently, spectra had to be measured with varying distances between target and instrument. With the laboratory measurements made on a gypsum sample, we identified different trends for increasing distances between sample and handheld instrument of Ar and Ca emission lines coming from the atmosphere and the sample, respectively. The Ar emission lines,

548 which contain no geochemical information regarding the present field inves-
549 tigation, can not be used for data normalization. Nevertheless, the approach
550 of rejecting spectra, which have a ratio between the integrated intensities
551 above and below 650 nm larger than one, was shown to be a useful indicator
552 for the quality of the spectra. We showed that the rejection threshold should
553 be chosen according to the spectra depending on their typical emission lines.
554 We found that LIBS data obtained with a distance of 40 mm or more between
555 sample and device are of reduced quality and not useful for further analysis.

556 For this study, a dedicated pre-processing of the data was necessary. First
557 approaches have shown that the influence of Ar emission lines coming from
558 the atmosphere on the PCA is strong and covers therefore information of
559 elemental variations. In order to avoid this, we masked all identified Ar
560 emission lines in the spectra. Subsequently, each spectrum was normalized
561 by its total emission intensity, mean centered, and its standard deviation was
562 scaled to unity.

563 For the data exploration with PCA, score and loading plots up to PC 6
564 were discussed. Clustering or trends related to the color of the layers were
565 not observed. However, for some individual layers similar trends for spectra
566 of the same layer could be seen. Each PC revealed correlations with several
567 combinations of elemental emission lines which allow therefore to do semi-
568 quantitative estimates of elemental abundances for each spectrum, at least
569 in relation to the other spectra. However, the loadings also show specific
570 correlations with emission lines that are influenced by varying line shapes
571 or line positions. From these correlations, deriving quantitative estimates
572 is challenging as it is complicated to relate them to elemental abundances.

573 Moreover, effects from a varying angle between instrument and sample (line
574 shifts) or self absorption are most likely responsible for these findings.

575 The layer-by-layer analysis of fitted emission lines revealed correlations
576 mainly between elements typical for felsic and mafic minerals in contrast to
577 an anti-correlation with Ca and F. This is in agreement with the expected
578 igneous minerals at the measurement site which are rich in alkalis. However,
579 as in the PCA, no clear relation of emission line intensities with the assigned
580 layer color was identified, except that Fe seems to be more abundant in most
581 red layers. Regarding minor and trace elements, several correlations could
582 be identified.

583 From the present study, it can be concluded that LIBS indeed is a pow-
584 erful elemental analysis technique even with the discussed challenges in field
585 applications. However, if possible, experimental conditions should be kept
586 as constant as possible between different measurements. The handheld LIBS
587 instrument used in this work has a high ease of use but is also limited in its
588 versatility because of the flat surface which has to be ideally put in full con-
589 tact with the sample surface. All in all, compositional variations of the ash
590 layers could be observed which was the objective of this study. The PCA as
591 well as the fitted emission lines served as useful tools for the data exploration
592 of the ash layers. The applied data pre-processing including the masking of
593 Ar emission lines lead to the best outcomes regarding the traceability of ele-
594 mental variations. In addition to the analysis, a better understanding of the
595 performance and limitations of the LIBS device was obtained which can help
596 to improve future field investigations using a handheld LIBS instrument but
597 also give input into instrument designs for robotic or human in-situ explo-

598 ration.

599 In general, based on this study, we recommend to do more than three mea-
600 surements at different positions on geological features which are suspected
601 to have a similar or even same elemental composition. 14% of our measure-
602 ments had to be rejected due to insufficient data quality which left not enough
603 data to derive statistically meaningful geochemical differences between the
604 layers. With more measurements in one layer, better estimates for the ho-
605 mogeneity of the layers and the reproducibility of the LIBS measurements
606 could have been possible. Another approach to improve the performance
607 of the instrument could be a change in the measurement mode: Instead of
608 integrating spectra of multiple induced plasmas, shot-to-shot measurements
609 could be done in order to obtain [data of the sample with increasing depth](#)
610 and to better understand underlying processes that influence the final LIBS
611 spectrum. This procedure could also provide a measure of the homogene-
612 ity of sample surfaces. Regarding the instrument, we want to emphasize
613 the importance to keep the sampling distance as small as possible and the
614 angle constant to maximize the performance and quality of the data when
615 measuring geological samples in the field. The sensitivity to the geometric
616 positioning arises from the configuration of this specific instrument and a
617 similar device for astronauts or hardware for an exploration rover should be
618 designed in a way that is more robust to these kinds of effects.

619 5. Conclusions and outlook

620 In the present study, LIBS data from in-field measurements of volcanic
621 ash layers using a handheld LIBS instrument were analyzed to evaluate the

622 easy of use of such LIBs devices for terrestrial and planetary geochemical
623 exploration. Additionally, measurements in the laboratory with the same
624 instrument were conducted in order to investigate the effect of varying dis-
625 tances between the sample and the device. An outcrop of volcanic ash on the
626 Eolian island Vulcano (Italy), which provides excellent planetary analog sites,
627 was measured within the framework of a Summer School held on the island
628 Vulcano. In this study, we focused on the performance of a handheld LIBS
629 device on geologically challenging and representative sample matrices and
630 designed and investigated various data analysis strategies. We found that
631 differences between the ash layers can be observed in the LIBS data. Cor-
632 relations of elemental emission intensities confirmed the shoshonitic-alkaline
633 character of the ashes. However, also challenges in field applications with
634 the handheld LIBS device were identified which concern mainly the varying
635 sample-instrument distance. Therefore, we give recommendations for future
636 field investigations using LIBS handheld instrumentation.

637 As mentioned in the beginning, samples were not only measured by LIBS
638 but also with VIS/NIR reflectance and Raman spectroscopy. In further stud-
639 ies, the combination of the data from these different spectroscopic techniques
640 is planned which could further improve sample identification as they provide
641 different types of data most likely enabling a more complete geological in-
642 terpretation. Furthermore, dedicated calibration models for the handheld
643 instrument in the particular conditions of field missions will be developed in
644 order to provide quantitative results from future explorations.

645 Acknowledgements

646 The Summer School held on Vulcano is an extension and continuation of
647 the successful previous four Summer Schools which were supported by the
648 Helmholtz Alliance Robotic Exploration of Extreme Environments (ROBEX)
649 and now generously supported by the EU Europlanet program. G.O. and
650 F.S. acknowledge funding by the Deutsche Forschungsgemeinschaft (DFG,
651 German Research Foundation) – Project-ID 263649064 – TRR 170. This is
652 TRR 170 Publication No. XX..

653 References

- 654 [1] David W. Hahn and Nicolás Omenetto. Laser-induced breakdown spec-
655 troscopy (LIBS), part II: Review of instrumental and methodological
656 approaches to material analysis and applications to different fields. *Ap-
657 plied Spectroscopy*, 66(4):347–419, 2012.
- 658 [2] Reinhard Noll, Holger Bette, Adriane Brysch, Marc Kraushaar, Ingo
659 Mönch, Laszlo Peter, and Volker Sturm. Laser-induced breakdown spec-
660 trometry - Applications for production control and quality assurance in
661 the steel industry. *Spectrochimica Acta - Part B Atomic Spectroscopy*,
662 56(6):637–649, 2001.
- 663 [3] Patrick Mauchien, Agnès Pailloux, and Thomas Vercouter. Applica-
664 tions of laser spectroscopy in nuclear research and industry. In *Laser
665 Spectroscopy for Sensing: Fundamentals, Techniques and Applications*,
666 pages 522–543. Woodhead Publishing, 2014.

- 667 [4] Maria Markiewicz-Keszycka, Xavier Cama-Moncunill, Maria P. Casado-
668 Gavalda, Yash Dixit, Raquel Cama-Moncunill, Patrick J. Cullen, and
669 Carl Sullivan. Laser-induced breakdown spectroscopy (LIBS) for food
670 analysis: A review. *Trends in Food Science and Technology*, 65:80–93,
671 2017.
- 672 [5] Asia Botto, Beatrice Campanella, Stefano Legnaioli, Marco Lezzerini,
673 Giulia Lorenzetti, Stefano Pagnotta, Francesco Poggialini, and Vincenzo
674 Palleschi. Applications of laser-induced breakdown spectroscopy in cul-
675 tural heritage and archaeology: A critical review. *Journal of Analytical*
676 *Atomic Spectrometry*, 34(1):81–103, 2019.
- 677 [6] Cécile Fabre. Advances in Laser-Induced Breakdown Spectroscopy anal-
678 ysis for geology: A critical review. *Spectrochimica Acta - Part B Atomic*
679 *Spectroscopy*, 166(February):105799, 2020.
- 680 [7] Russell S. Harmon, Richard E. Russo, and Richard R. Hark. Appli-
681 cations of laser-induced breakdown spectroscopy for geochemical and
682 environmental analysis: A comprehensive review. *Spectrochimica Acta*
683 *- Part B Atomic Spectroscopy*, 87:11–26, 2013.
- 684 [8] Giorgio S. Senesi. Laser-Induced Breakdown Spectroscopy (LIBS) ap-
685 plied to terrestrial and extraterrestrial analogue geomaterials with em-
686 phasis to minerals and rocks. *Earth-Science Reviews*, 139:231–267, 2014.
- 687 [9] S Maurice, R C Wiens, M Saccoccio, B Barraclough, O Gasnault,
688 O Forni, N Mangold, D Baratoux, S Bender, G Berger, J Bernardin,
689 M Berthé, N Bridges, D Blaney, M Bouyé, P Caïs, B Clark, S Clegg,

690 A Cousin, D Cremers, A Cros, L Deflores, C Derycke, B Dingler, G Dro-
691 mart, B Dubois, M Dupieux, E Durand, L D’Uston, C Fabre, B Faure,
692 A Gaboriaud, T Gharsa, K Herkenhoff, E Kan, L Kirkland, D Kouach,
693 J L Lacour, Y Langevin, J Lasue, S Le Mouélic, M Lescure, E Lewin,
694 D Limonadi, G Manhès, P Mauchien, C McKay, P Y Meslin, Y Michel,
695 E Miller, H E Newsom, G Orttner, A Paillet, L Parès, Y Parot, R Pérez,
696 P Pinet, F Poitrasson, B Quertier, B Sallé, C Sotin, V Sautter, H Séran,
697 J J Simmonds, J B Sirven, R Stiglich, N Striebig, J J Thocaven, M J
698 Toplis, and D Vaniman. The ChemCam instrument suite on the Mars
699 Science Laboratory (MSL) rover: Science objectives and mast unit de-
700 scription. *Space Science Reviews*, 170(1-4):95–166, 2012.

701 [10] Roger C. Wiens, Sylvestre Maurice, Bruce Barracough, Muriel Saccoc-
702 cio, Walter C. Barkley, James F. Bell, Steve Bender, John Bernardin, Di-
703 ana Blaney, Jennifer Blank, Marc Bouyé, Nathan Bridges, Nathan Bult-
704 man, Phillippe Caïs, Robert C. Clanton, Benton Clark, Samuel Clegg,
705 Agnes Cousin, David Cremers, Alain Cros, Lauren Deflores, Dorothea
706 Delapp, Robert Dingler, Claude D’Uston, M. Darby Dyar, Tom Elliott,
707 Don Enemark, Cecile Fabre, Mike Flores, Olivier Forni, Olivier Gas-
708 nault, Thomas Hale, Charles Hays, Ken Herkenhoff, Ed Kan, Laurel
709 Kirkland, Driss Kouach, David Landis, Yves Langevin, Nina Lanza,
710 Frank Larocca, Jeremie Lasue, Joseph Latino, Daniel Limonadi, Chris
711 Lindensmith, Cynthia Little, Nicolas Mangold, Gerard Manhes, Patrick
712 Mauchien, Christopher McKay, Ed Miller, Joe Mooney, Richard V.
713 Morris, Leland Morrison, Tony Nelson, Horton Newsom, Ann Ollila,
714 Melanie Ott, Laurent Pares, René Perez, Franck Poitrasson, Cheryl

- 715 Provost, Joseph W. Reiter, Tom Roberts, Frank Romero, Violaine Saut-
716 ter, Steven Salazar, John J. Simmonds, Ralph Stiglich, Steven Storms,
717 Nicolas Striebig, Jean Jacques Thocaven, Tanner Trujillo, Mike Ulibarri,
718 David Vaniman, Noah Warner, Rob Waterbury, Robert Whitaker,
719 James Witt, and Belinda Wong-Swanson. The ChemCam instrument
720 suite on the Mars Science Laboratory (MSL) rover: Body unit and com-
721 bined system tests. *Space Science Reviews*, 170(1-4):167–227, 2012.
- 722 [11] S. Maurice, S. M. Clegg, R. C. Wiens, O. Gasnault, W. Rapin, O. Forni,
723 A. Cousin, V. Sautter, N. Mangold, L. Le Deit, M. Nachon, R. B. An-
724 derson, N. L. Lanza, C. Fabre, V. Payré, J. Lasue, P. Y. Meslin, R. J.
725 Lèveillé, B. L. Barraclough, P. Beck, S. C. Bender, G. Berger, J. C.
726 Bridges, N. T. Bridges, G. Dromart, M. D. Dyar, R. Francis, J. Fry-
727 denvang, B. Gondet, B. L. Ehlmann, K. E. Herkenhoff, J. R. Johnson,
728 Y. Langevin, M. B. Madsen, N. Melikechi, J. L. Lacour, S. Le Mouélic,
729 E. Lewin, H. E. Newsom, A. M. Ollila, P. Pinet, S. Schröder, J. B. Sir-
730 ven, R. L. Tokar, M. J. Toplis, C. D’Uston, D. T. Vaniman, and A. R.
731 Vasavada. ChemCam activities and discoveries during the nominal mis-
732 sion of the Mars Science Laboratory in Gale crater, Mars. *Journal of*
733 *Analytical Atomic Spectrometry*, 31(4):863–889, 2016.
- 734 [12] Andrew K. Knight, Nancy L. Scherbarth, David A. Cremers, and
735 Monty J. Ferris. Characterization of laser-induced breakdown spec-
736 troscopy (LIBS) for application to space exploration. *Applied Spec-*
737 *troscopy*, 54(3):331–340, 2000.
- 738 [13] Roger C. Wiens, Sylvestre Maurice, and Fernando Rull Perez. The

- 739 SuperCam Remote Sensing Instrument Suite for the Mars 2020 Rover:
740 A Preview. *Spectroscopy*, 32(5):50–55, 2017.
- 741 [14] A.S. Laxmiprasad, V.L.N. Sridhar Raja, Surya Menon, Adwaita
742 Goswami, M.V.H. Rao, and K.A. Lohar. An in situ laser induced break-
743 down spectroscopy (libs) for chandrayaan-2 rover: Ablation kinetics and
744 emissivity estimations. *Advances in Space Research*, 52(2):332 – 341,
745 2013. Lunar Exploration - II.
- 746 [15] X. Ren, T. N. Cai, D. W. Liu, J. J. Liu, H. B. Zhang, Q. Fu, Z. B.
747 Zhang, and W. M. Xu. Preliminary Scientific Exploration Programs for
748 Mars Surface Composition Detection Package of China’s First Mars Ex-
749 ploration. In *12th European Planetary Science Congress*, page Abstract
750 #759, Berlin, Germany, 2018.
- 751 [16] J. Lasue, R. C. Wiens, S. M. Clegg, D. T. Vaniman, K. H. Joy,
752 S. Humphries, A. Mezzacappa, N. Melikechi, R. E. McInroy, and S. Ben-
753 der. Remote laser-induced breakdown spectroscopy (LIBS) for lunar
754 exploration. *Journal of Geophysical Research E: Planets*, 117(1), 2012.
- 755 [17] S. G. Pavlov, S. Schröder, I. Rauschenbach, E. K. Jessberger, and H. W.
756 Hübers. Low-energy laser induced breakdown spectroscopy for in-situ
757 space missions to solar system bodies without atmospheres. *Planetary
758 and Space Science*, 2012.
- 759 [18] S. M. Clegg, M. D. Dyar, R. T. Newell, C. G. Peterson, D. S. DeCroix,
760 B. S. Okhuysen, S. K. Sharma, S. Maurice, R. C. Wiens, and L. S.
761 Glaze. Venus elemental and mineralogical camera (vemcam). In *49th*

- 762 *Lunar and Planetary Science Conference*, page Abstract #2676, The
763 Woodlands, USA, 2018. Lunar and Planetary Institute.
- 764 [19] David A Cremers and Leon J Radziemski. *Handbook of laser induced*
765 *breakdown spectroscopy*. Wiley, Chichester, 2. ed. edition, 2013.
- 766 [20] W. D. Hahn and N. Omenetto. Laser-Induced Breakdown Spectroscopy
767 (LIBS), Part I: Review of Basic Diagnostics and Plasma-Particle Inter-
768 actions: Still-Challenging Issues Within the Analytical Plasma Commu-
769 nity. *Appl. Spectrosc.*, 64:335A–366A, 2010.
- 770 [21] J. El Haddad, L. Canioni, and B. Bousquet. Good practices in LIBS
771 analysis: Review and advices. *Spectrochimica Acta Part B: Atomic Spec-*
772 *troscopy*, 101:171–182, nov 2014.
- 773 [22] Sarah C. Jantzi, Vincent Motto-Ros, Florian Trichard, Yuri Markushin,
774 Nouredine Melikechi, and Alessandro De Giacomo. Sample treatment
775 and preparation for laser-induced breakdown spectroscopy. *Spectrochim-*
776 *ica Acta Part B: Atomic Spectroscopy*, 115:52–63, jan 2016.
- 777 [23] R Tessadri. Introduction to the mineralogical sciences. pt 3: An-
778 alytical techniques for elemental analysis of minerals. In *UN-*
779 *ESCO—Encyclopedia of Life Support Systems EOLSS*. on-line, publi-
780 cation, www.eolss.net, 2003.
- 781 [24] John L Campbell, Glynis M Perrett, Ralf Gellert, Stefan M An-
782 drushenko, Nicholas I Boyd, John A Maxwell, Penelope L King, and
783 Céleste DM Schofield. Calibration of the mars science laboratory alpha

- 784 particle x-ray spectrometer. *Space Science Reviews*, 170(1-4):319–340,
785 2012.
- 786 [25] Elisabetta Tognoni and Gabriele Cristoforetti. Signal and noise in Laser
787 Induced Breakdown Spectroscopy: An introductory review. *Optics and*
788 *Laser Technology*, 79(May):164–172, 2016.
- 789 [26] J.-B. Sirven, B. Bousquet, L. Canioni, and L. Sarger. Laser-Induced
790 Breakdown Spectroscopy of Composite Samples: Comparison of Ad-
791 vanced Chemometrics Methods. *Analytical Chemistry*, 78(5):1462–1469,
792 2006.
- 793 [27] G De Astis, F Lucchi, P Dellino, L La Volpe, C A Tranne, M L Frezzotti,
794 and A Peccerillo. Chapter 11 Geology, volcanic history and petrology
795 of Vulcano (central Aeolian archipelago). *Geological Society, London,*
796 *Memoirs*, 37(1):281 LP – 349, 2013.
- 797 [28] Stefano Rossi, Maurizio Petrelli, Daniele Morgavi, Francesco P. Vet-
798 ere, Renat R. Almeev, Rebecca L. Astbury, and Diego Perugini. Role
799 of magma mixing in the pre-eruptive dynamics of the Aeolian Islands
800 volcanoes (Southern Tyrrhenian Sea, Italy). *Lithos*, 324-325:165–179,
801 2019.
- 802 [29] K. Stephan, S. Schröder, M. Baqué, K. Rammelkamp, J. Haber,
803 I. Varatharajan, G. Ortenzi, A. Pisello, R. Pasek, F. Sohl, R. Jaumann,
804 L. Thomson, and V. Unnithan. Multi-spectral investigation of vol-
805 canic deposits and their alteration processes on Vulcano/ Italy. In *13th*

- 806 *European Planetary Science Congress*, page Abstract #2062, Geneva,
807 Switzerland, 2019.
- 808 [30] K. Stephan, S. Schröder, M. Baqué, K. Rammelkamp, J. Haber,
809 I. Varatharajan, G. Ortenzi, A. Pisello, R. Pasek, F. Sohl, R. Jaumann,
810 L. Thomson, and V. Unnithan. Multi-spectral investigation of plane-
811 tary analog material in extreme environments - alteration products of
812 volcanic deposits of Vulcano/Italy. In *51th Lunar and Planetary Science*
813 *Conference*, page Abstract #2411, The Woodlands, USA, 2020.
- 814 [31] Lionel Wilson. Volcanism in the solar system. *Nature Geoscience*,
815 2(6):389, 2009.
- 816 [32] Brendan Connors, Andrew Somers, and David Day. Application of
817 Handheld Laser-Induced Breakdown Spectroscopy (LIBS) to Geochem-
818 ical Analysis. *Applied Spectroscopy*, 70(5):810–815, 2016.
- 819 [33] Russell S. Harmon, Richard R. Hark, Chandra S. Throckmorton, Eu-
820 gene C. Rankey, Michael A. Wise, Andrew M. Somers, and Leslie M.
821 Collins. Geochemical Fingerprinting by Handheld Laser-Induced
822 Breakdown Spectroscopy. *Geostandards and Geoanalytical Research*,
823 41(4):563–584, 2017.
- 824 [34] Russell S. Harmon, Chandra S. Throckmorton, Richard R. Hark, Jen-
825 nifer L. Gottfried, Gerhard Wörner, Karen Harpp, and Leslie Collins.
826 Discriminating volcanic centers with handheld laser-induced breakdown
827 spectroscopy (LIBS). *Journal of Archaeological Science*, 98(July):112–
828 127, 2018.

- [35] Y. Foucaud, C. Fabre, B. Demeusy, I. V. Filippova, and L. O. Filippov. Optimisation of fast quantification of fluorine content using handheld laser induced breakdown spectroscopy. *Spectrochimica Acta - Part B Atomic Spectroscopy*, 158:105628, 2019.
- [36] Cai R. Ytsma, Christine A. Knudson, M. Darby Dyar, Amy C. McAdam, Danielle D. Michaud, and Lindsey M. Rollosso. Accuracies and detection limits of major, minor, and trace element quantification in rocks by portable laser-induced breakdown spectroscopy. *Spectrochimica Acta Part B: Atomic Spectroscopy*, 171(July):105946, sep 2020.
- [37] M. H. Yant, K. W. Lewis, A. H. Parker, S. M. Hörst, A. C. McAdam, and C. A. Knudson. Project espresso: Exploration roles of handheld libs at the potrillo volcanic field. In *50th Lunar and Planetary Science Conference*, page Abstract #2645, Houston, 2019. Lunar and Planetary Institute.
- [38] Giorgio S. Senesi, Russell S. Harmon, and Richard R. Hark. Field-portable and handheld laser-induced breakdown spectroscopy: Historical review, current status and future prospects. *Spectrochimica Acta Part B: Atomic Spectroscopy*, 175(October 2020):106013, jan 2021.
- [39] Bernard Foing. Overview of moon village global activities & lunar explorers tribute. In *EGU General Assembly Conference Abstracts*, volume 20, page 18534, 2018.
- [40] Yasuo Iida. Effects of atmosphere on laser vaporization and excitation

- 851 processes of solid samples. *Spectrochimica Acta Part B: Atomic Spec-*
852 *troscopy*, 45(12):1353–1367, 1990.
- 853 [41] R.J. Lasheras, C. Bello-Gálvez, and J.M. Anzano. Quantitative anal-
854 ysis of oxide materials by laser-induced breakdown spectroscopy with
855 argon as an internal standard. *Spectrochimica Acta Part B: Atomic*
856 *Spectroscopy*, 82:65–70, 2013.
- 857 [42] A. De Giacomo, M. Dell’Aglio, R. Gaudioso, S. Amoruso, and O. De
858 Pascale. Effects of the background environment on formation, evolution
859 and emission spectra of laser-induced plasmas. *Spectrochimica Acta Part*
860 *B: Atomic Spectroscopy*, 78:1–19, 2012.
- 861 [43] Jörg Hermann, Christoph Gerhard, Emanuel Axente, and Christophe
862 Dutouquet. Comparative investigation of laser ablation plumes in air
863 and argon by analysis of spectral line shapes: Insights on calibration-
864 free laser-induced breakdown spectroscopy. *Spectrochimica Acta Part*
865 *B: Atomic Spectroscopy*, 100:189–196, 2014.
- 866 [44] S. Schröder, K. Rammelkamp, D.S. Vogt, O. Gasnault, and H.-W.
867 Hübers. Contribution of a martian atmosphere to laser-induced break-
868 down spectroscopy (LIBS) data and testing its emission characteristics
869 for normalization applications. *Icarus*, 325(December 2018):1–15, 2019.
- 870 [45] A. Kramida, Yu. Ralchenko, J. Reader, and and NIST ASD Team.
871 NIST Atomic Spectra Database (ver. 5.7.1), [Online]. Available:
872 <https://physics.nist.gov/asd> [2020, March 12]. National Institute
873 of Standards and Technology, Gaithersburg, MD., 2019.

- [46] G. De Astis, L. La Volpe, A. Peccerillo, and L. Civetta. Volcanological and petrological evolution of Vulcano island (Aeolian Arc, southern Tyrrhenian Sea). *Journal of Geophysical Research: Solid Earth*, 102(B4):8021–8050, 1997.
- [47] Raffaella Fusillo, Federico Di Traglia, Anna Gioncada, Marco Pistolesi, Paul J. Wallace, and Mauro Rosi. Deciphering post-caldera volcanism: insight into the Vulcanello (Island of Vulcano, Southern Italy) eruptive activity based on geological and petrological constraints. *Bulletin of Volcanology*, 77(9), 2015.
- [48] M. Gaft, L. Nagli, N. Eliezer, Y. Groisman, and O. Forni. Elemental analysis of halogens using molecular emission by laser-induced breakdown spectroscopy in air. *Spectrochimica Acta - Part B Atomic Spectroscopy*, 98:39–47, 2014.
- [49] Olivier Forni, Michael Gaft, Michael J. Toplis, Samuel M. Clegg, Sylvestre Maurice, Roger C. Wiens, Nicolas Mangold, Olivier Gasnault, Violaine Sautter, Stéphane Le Mouélic, Pierre Yves Meslin, Marion Nachon, Rhonda E. McInroy, Ann M. Ollila, Agnès Cousin, John C. Bridges, Nina L. Lanza, and Melinda D. Dyar. First detection of fluorine on Mars: Implications for Gale Crater’s geochemistry. *Geophysical Research Letters*, 42(4):1020–1028, 2015.
- [50] D.S. Vogt, S. Schröder, K. Rammelkamp, P.B. Hansen, S. Kubitza, and H.-W. Hübers. CaCl and CaF emission in LIBS under simulated Martian conditions. *Icarus*, 335:113393, 2020.

- 897 [51] Igor B. Gornushkin, Leslie A. King, Ben W. Smith, Nicolás Omenetto,
898 and James D. Winefordner. Line broadening mechanisms in the low
899 pressure laser-induced plasma. *Spectrochimica acta, Part B: Atomic*
900 *spectroscopy*, 54(8):1207–1217, 1999.
- 901 [52] Koo Hendrik Kurniawan, May On Tjia, and Kiichiro Kagawa. Review of
902 Laser-Induced Plasma, Its Mechanism, and Application to Quantitative
903 Analysis of Hydrogen and Deuterium. *Applied Spectroscopy Reviews*,
904 49(5):323–434, 2014.
- 905 [53] D. S. Vogt, K. Rammelkamp, S. Schröder, and H. W. Hübers. Molecular
906 emission in laser-induced breakdown spectroscopy: An investigation of
907 its suitability for chlorine quantification on Mars. *Icarus*, 302:470–482,
908 2018.

